Available online at www.sciencedirect.com
SCIENCE DIRECT
Cement and Concrete Research 36 (2006) 337 – 345
Cement and Concrete Research

Measurement of aggregate interfacial porosity in complex, multi-phase aggregate concrete: Binary mask production using backscattered electron, and energy dispersive X-ray images

Martin K. Head *, Nick R. Buenfeld

Department of Civil and Environmental Engineering, Imperial College London Imperial College Road, London, SW7 2BU, UK

Received 3 March 2004; accepted 19 September 2005

Abstract

This paper presents for the first time a method for the accurate segmentation of complex (multi-phase) natural aggregate particles, from greyscale backscattered electron images (BEI) of hardened concrete, so that interfacial porosity may be measured. Energy dispersive X-ray (EDX) spectra are collected from phases present in aggregate particles to identify the most abundant and therefore useful elements to be captured during later mapping. Appropriately captured energy dispersive X-ray dot maps are used to progressively construct a multi-phase composite aggregate binary mask, for aggregate particles composed of more than one mineral. The mask image is then re-processed in combination with the backscattered image, to produce an accurate hardened cement paste (HCP) porosity mask, which is used to measure the distribution of interfacial porosity around aggregate particles.

Keywords: Scanning electron microscope; Energy dispersive X-rays; Image analysis; Aggregate mineralogy

1. Introduction

Traditional methods for measuring hardened concrete coarse aggregate interfacial porosity frequently include the use of backscattered electron images (BEI) captured with a scanning electron microscope (SEM) [1,2]. Images are segmented by greyscale thresholding to produce binary images of regions of interest (ROI's), which is a relatively straightforward operation when all features of interest are clearly greyscale contrasted. However many concretes are manufactured with natural aggregates comprised of multiple phases (naturally occurring minerals), which very often share the same, or very similar, backscattered coefficients as phases developed within the hardened cement paste (HCP). In this situation segmentation is not straightforward as features and phases that lie within both coarse aggregate particles, and HCP, are selected together during thresholding procedures.

This is particularly true for the calcium–silicate–hydrate (C–S–H) fraction of the HCP, with silica-rich mineral phases such as quartz and feldspars (fine and coarse aggregate). Calcium-rich phases can also be found as inclusions in the aggregate (e.g. calcite and feldspars), and share very similar backscattered electron signal coefficients to anhydrous fractions of cement particles. Other mineral phases may be (relatively) rich in aluminium (e.g. feldspars), iron (e.g. ore minerals) or alkali ions (e.g. feldspars), all of which may produce very similar backscattered coefficients to HCP phases such as calcium hydroxide (CH) or even ettringite. Simply contrasting the image during image capture may not be sufficient to allow accurate segmentation. This paper demonstrates a method for constructing an accurate aggregate binary mask that can be used for later measurement of interfacial porosity on a BEI.

A concrete was prepared in the laboratory using a w/c ratio of 0.325 with ordinary Portland cement, quartz fine aggregate, and dolerite coarse aggregate in the ratio of 1:2:3. Hydration was halted at 28 days by freeze drying, and the specimen was resin impregnated under vacuum. After curing of the resin, the specimen was trimmed to a usable size and one of the flat surfaces was ground with progressively finer grades of SiC paper, so that a final surface finish equivalent to a 10 μm

* Corresponding author. Tel.: +44 207 594 5956; fax: +44 207 225 2716.
E-mail address: m.head@imperial.ac.uk (M.K. Head).

0008-8846/$ - see front matter © 2005 Elsevier Ltd. All rights reserved.
doi:10.1016/j.cemconres.2005.09.007

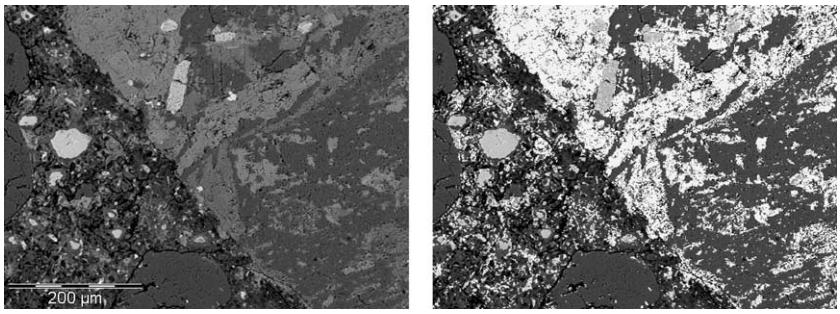

a) Original BEI captured at x200 b) Application of threshold values 104 - 131

Fig. 1. Initial attempt at segmentation of aggregate mid-range greyscale values.

diamond particle size was achieved. The specimen was then glued to a glass slide with an araldite-type resin. After hardening, excess material was removed with a fine cut-off saw, and the new surface was ground to give a material thickness of approximately 45 µm. Final, fine grinding was performed (as previous) prior to polishing. The surface was then polished with progressively finer diamond polishing compounds to a final tolerance of 1 µm, and the specimen was stored in a dessicator with dry silica gel until needed for analysis.

In Fig. 1, simple thresholding of coarse aggregate mid-range greyscale values has been attempted. However, this has only resulted in a partial selection of the coarse aggregates' mineral phases. At least two other phases that are lighter and darker than the selected range have been excluded. Additionally, unwanted areas of the HCP have been included. If the greyscale selection range was extended to include the aggregate phases, large areas of the HCP would also be segmented, resulting in a completely erroneous binary mask. Fig. 1b shows that the segmented interface between the coarse aggregate and HCP is highly fragmented and has areas that overlap into the HCP. This can be observed towards the lower edge of the image where a more dense hydrate phase (probably calcium hydroxide) has developed in virtual contact with a mid-grey range, coarse aggregate mineral phase.

It is clear, therefore, that a more accurate and reliable way to produce a coarse aggregate binary mask is needed. This can be achieved through the use of EDX dot maps, collected in tandem with a BEI, and is an effective way of mapping elements found in the constituent fractions of the BEI. These elemental X-ray images can be used in image analysis algorithms to construct an accurate binary mask, which can then be superimposed on the BEI for measurement purposes. Bäckström and Hansen [3] employed this method to map interstitial phases in sulphate-resisting cement clinker. It was later adapted by Brough and Atkinson [4] who developed a procedure to allow automated identification of the aggregate paste ITZ in mortars comprised of silica sand and Portland cement or alkali activated slag cement pastes. More recently, Stutzman [5] has applied the technique of combined BEI and EDX imaging to the study of bulk phase abundance and surface area of phases in clinker and cement.

In order to apply this technique to the identification and mapping of aggregate (coarse or fine) phases (minerals) and interfaces in concrete specimens, it is necessary to have a prior knowledge of chemical compositions of the phases. For this study the adopted methodology was to use an EDX spectrum, captured from the coarse aggregate, in order to determine the most useful elements for later dot mapping. The captured spectrum is presented in Fig. 2, where it can be seen that 10 elements (O, Na, Mg, Al, Si, K, Ca, Ti, Mn, and Fe) are present in sufficient amounts to create clear peaks in the data.

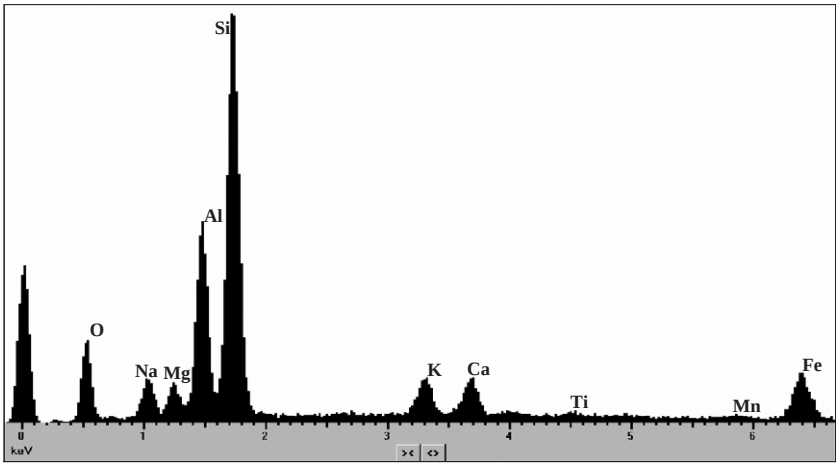

Fig. 2. EDX spectrum collected from coarse aggregate particle.

2. Data capture: collection of backscattered electron and elemental X-ray images

The images presented below (Fig. 3) were captured on a JEOL 5410 LV scanning electron microscope. The microscope is fitted with an Oxford Instruments' LINK ISIS micro analyser for the capture and processing of energy dispersive X-rays. X-ray data for 30 data sets were captured over 30 frames for each set (the example set provided in Fig. 3, was captured over 100 frames) on an image resolution setting of 512×384 pixels and a magnification of $\times 200$ giving a field of view of approximately 600 μm. This maximum resolution setting is less than ideal but is limited by the hardware resources of the system. In the event, manganese (Mn) and titanium (Ti) elements were only present as trace, and would not contribute much to later image analysis operations. Their corresponding X-ray images were therefore not captured allowing for the capture of more important element X-ray images at the highest available resolution. Oxygen (O) and magnesium (Mg) were also not captured for analysis. As can be seen in Fig. 2, the data peak for aluminium (Al) is stronger than for Mg, and as Mg mainly occurred in phases that also included Al, the capture of an Mg X-ray image was felt to be unnecessary. The removal of O was due to its relative abundance in all the phases.

The magnification was chosen to aid the visualisation of different phases within the field of view. Higher magnifications are often used for image capture (e.g. $\times 500$) where the resolving power of the microscope is optimised during image capture. During data collection, a backscattered electron image can be captured at the same time as the EDX element images, whereby each pixel of the backscattered image can be directly related to corresponding pixels on each of the accompanying X-ray images. Therefore, the final choice of image capture was a backscattered electron image and X-ray images for Na, Ca, Al, Si, K, and Fe (see Fig. 3).

3. Image processing

Image processing was performed using analySIS®, a dedicated high end quantitative image analysis software package. Images may be filtered to remove signal noise and other image features, such as surface damage incurred during specimen processing. Using a greyscale threshold function,

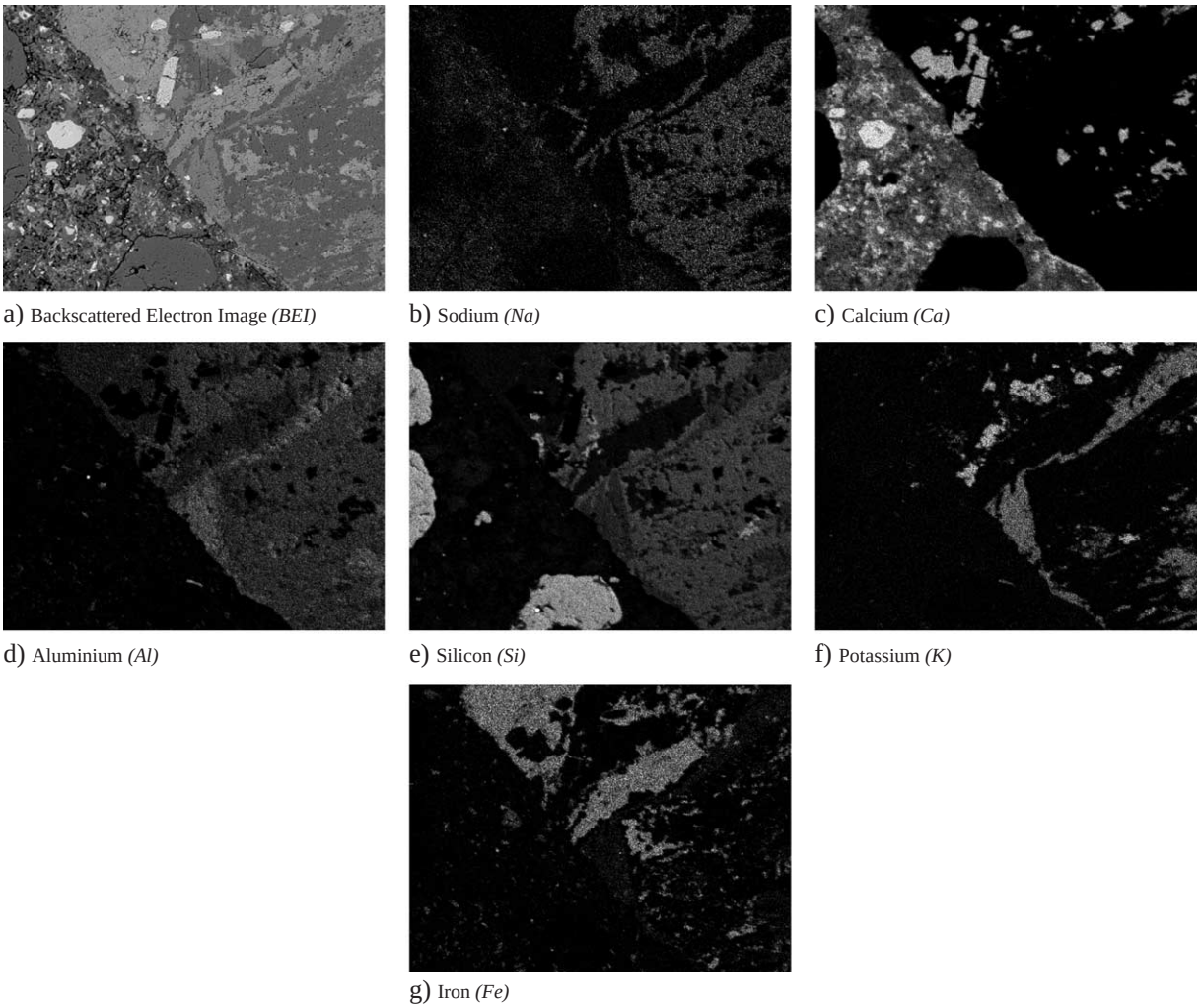

Fig. 3. BEI and EDX images for hardened concrete with basalt coarse aggregate (fields of view approx. 600 μm).

objects of interest can be segmented to produce binary image masks. The accuracy of these 'binary masks' controls the subsequent accuracy of measurement operations; consequently, filtering was kept to a minimum to preserve as many features of the coarse aggregate interface as possible.

3.1. Construction of composite aggregate binary mask

Having identified the most useful elements comprising the coarse aggregate mineral phases, their X-ray images were used in combination to construct the coarse aggregate fraction of the BEI. The Si, Fe, and Al images were added together to give a composite image as shown in Fig. 4a, where the aggregate interface is clearly defined for most of its length. Most of the black areas located within the coarse aggregate particle indicate where phases rich in calcium (Ca) have not been included. If the calcium image in its entirety were to be added, the aggregate paste interface would be virtually lost rendering thresholding operations extremely difficult at best. This is also true for aggregates that have a very high content of Ca such as limestone, where little difference between the Ca intensity in both aggregate and HCP is observed. In this situation, it may be possible to make more use of elements of lower abundance that may be present within the aggregate, as opposed to discarding them. Image algorithms can also be used to combine minor element X-ray images, such that they become useful for image segmentation routines. For example, X-ray images may be combined to form element 'ratio' images that can be easily segmented, and is similar in concept to the method adopted by Brough and Atkinson [4] in their study of Portland, or, alkali-activated slag cement pastes. Here, a composite image was created by using the silica (Si) and Ca X-ray images in the form Si-2 × Ca, which altered the relative ratios of Si and Ca in the aggregate and HCP areas of the composite image. A Si/Ca ratio map was produced that contrasted the paste area of the image with the silica-rich aggregate, identifying the aggregate interface and aiding subsequent thresholding operations. The image analysis routines developed to analyse the 30 image data sets here, were written to allow the flexible combination of any of the captured elemental X-ray images, to contribute towards construction of the best possible merged compound coarse aggregate image.

To this end, the method can also help to isolate Ca-rich phases that are in contact with longer lengths of the aggregate interface. In order to fill the 'holes' within the coarse aggregate shown in Fig. 4a, it is necessary to perform further image processing on the Ca image to isolate aggregate only areas, which can then be combined with the above semi-complete composite image. This was achieved by employing standard particle separation methods such as binarisation, followed by region reduction (separation by erosion), and reconstruction (dilation) without rejoining of the original features. Unwanted areas can then be simply removed from the image, and the result is shown in Fig. 4b. In Fig. 4c, the aggregate only calcium is combined with the previously constructed image (Fig. 4a) to complete the coarse aggregate phase composite; the remaining black areas represent surface damage that has been in-filled with resin.

The image presented in Fig. 4c is now almost contrasted well enough to allow accurate segmentation of the coarse aggregate interface. However, an accumulation of pixel intensities during addition of the four X-ray images has resulted in image noise which does not produce a clear histogram for thresholding purposes. To better define the peaks prior to image segmentation, a simple 'lowpass' averaging filter was applied to the image. This filter works by averaging the greyscale values of neighbouring pixels located around a central, operational pixel. The effect is to slightly blur image features as their greyscale values move closer together (smoothing the image) but differences between dark and light areas are emphasized resulting in better peak definition. Histograms plotted from both the un-filtered and filtered image data of Fig. 4c are shown in Fig. 5a. Note that the pure white pixel peak (value 255) in the un-filtered data has been removed as part of the averaging process. The pixel count for this peak is actually 6143, but all of these pixels have been incorporated into the 'bright' value peak in the filtered data histogram (approx. greyscale value 175), helping to improve peak definition and separation. From this, a segmentation threshold value of 110 was selected, and the resulting binary image is shown in Fig. 5b.

Thresholding at these greyscale values optimised the reduction of image noise and artefact inclusion. Even so, as can be observed in Fig. 5b, small amounts of noise and unwanted particles are still present in the image (small black

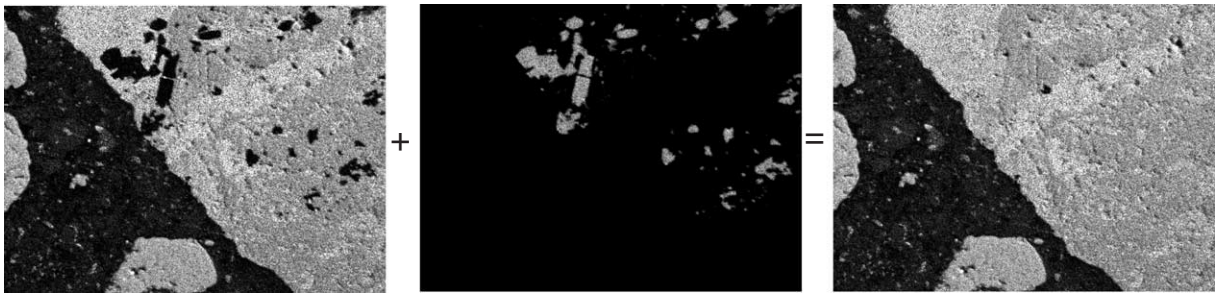

a) Si + Fe + Al composite image

b) Coarse aggregate, Ca dominant phases

c) Final merged X-ray image for coarse aggregate phases (Si + Fe + Al + Ca)

Fig. 4. Final stages of compiling coarse aggregate composite image from element X-ray images (fields of view approx. 600 μm).

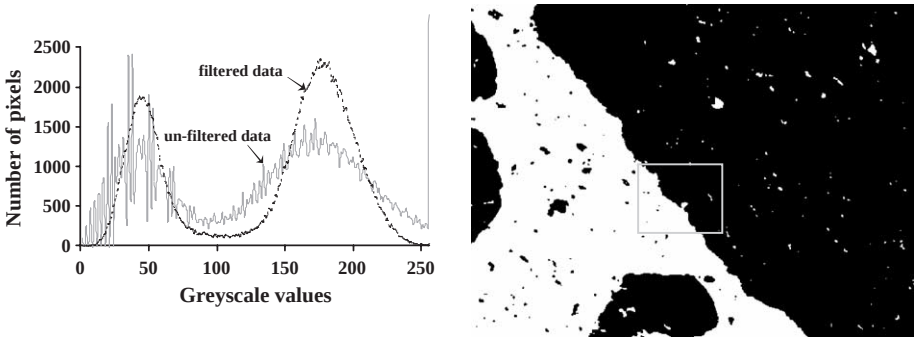

a) Image datahistograms (from Fig. 4c)

b) Binary image produced from filtered image data (see text for explanation of rectangle)

Fig. 5. Histograms for compound un-filtered and filtered images, and subsequently thresholded binary image-generated from filtered data (note that in (a), the *y*-axis has been reset to a maximum of 2500 pixel counts).

'holes' and small white specks). These were removed by a combination of logical morphology operations. The binary image was first subjected to a hole-filling filter which removed the particles in the black regions of the image, then the image was inverted and the hole-filling procedure was repeated. To remove noise at the interface, a 'close' filter was applied. This is a combined dilate and erosion operation using a hexagonal-based filter of size 3 (see Fig. 7). The image was then inverted and subjected to a further 'close' function and then a final inversion. The end product is a 'clean' binary image which is ready for image analysis work. A section of the image has been magnified (rectangle on Fig. 5b) and presented in Fig. 6a–h to demonstrate the iterative effect of this procedure.

The use of many image processing steps is normal in routine image analysis procedures and can be much more complex than illustrated here. As long as the number and type of operations are carefully monitored and balanced, accuracy of the originally segmented regions can be maintained.

A hexagonal morphological filter is based on a definition of six-connectivity as would be the case in a hexagonal pixel matrix, where each pixel is connected to horizontal, and vertical neighbours, but to only one pair of diagonal neighbours (which lie on the same diagonal). It is therefore possible to define 14 separate possibilities for surrounding the central operational pixel with neighbouring pixel values of 1 or 0, creating a very flexible structuring element for morphological filtering. Ordinarily, structure elements based on a square pixel matrix consider four- or eight-connectivity, limiting the available functions of the morphological filter. The hexagonal arrangement can be simulated in a square data set by assuming that each row is shifted by half a pixel, as in the case of the software used in this study. Selection of neighbouring pixels will therefore depend on whether the central pixel is located in an 'even' or 'odd' image line (Fig. 7c–e). A strong advantage with the hexagonal structuring element in its smallest form (3×3 pixels) is its' ability to retain the original shape of

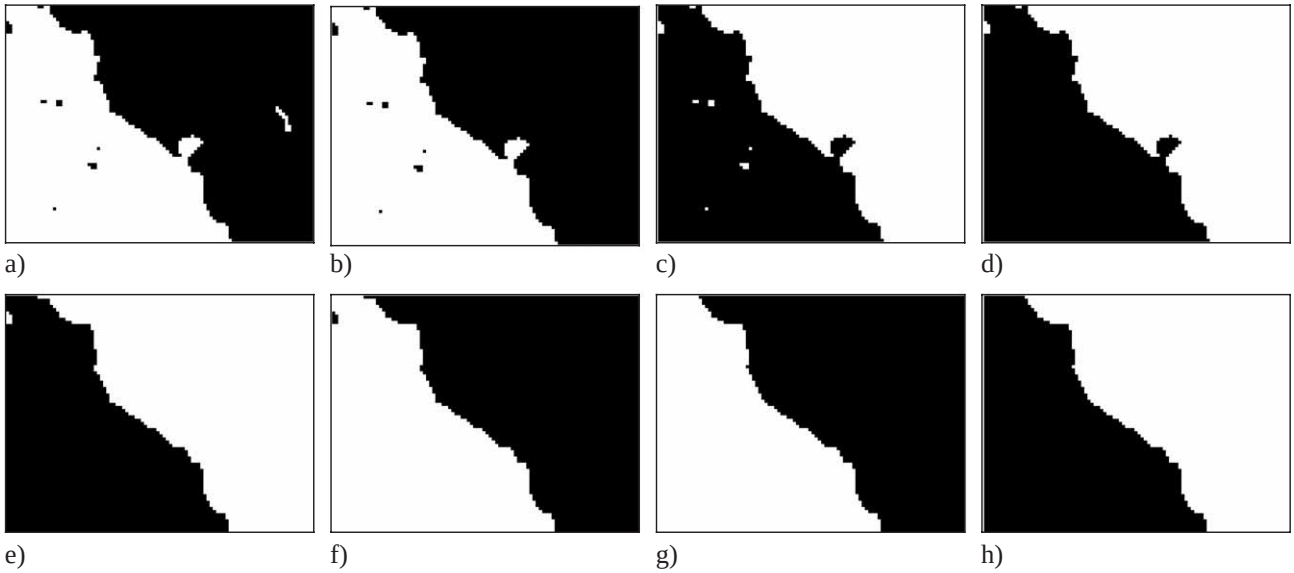

Fig. 6. a) Zoomed region of Fig. 5b showing various artefacts and noise, b) hole-filling to remove noise in dark area of image, c) inverted image of b), d) hole-filling on inverted image, e) 'close' morphological operation with hexagonal filter of size 3, f) inverted image of e), g) 'close' operation performed on inverted image, h) final inverted image of g).

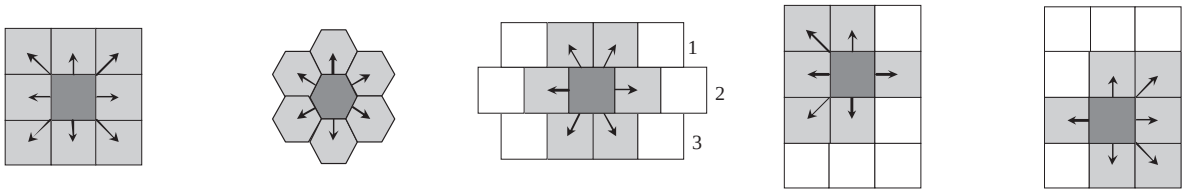

a) Square pixel matrix showing eight-connectivity of central pixel.

b) Hexagonal pixel matrix showing six-connectivity of central pixel.

c) Square pixel matrix with each row (1-3) offset by half a pixel, and six-connectivity of pixels defined by hexagonal structure element.

d) Interpretation of structure by software operating on a square pixel matrix. Central pixel is located on an 'even' (2) image line.

e) Interpretation of structure by software operating on a square pixel matrix. Central pixel is located on an'odd' (3) image line.

Fig. 7. Diagrams of morphological structure elements (filter size=pixels). (a), (d), and (e) modified from analySIS® image analysis software user guide; (b) and (c) adapted from on-line information provided by National Instruments—see http://zone.ni.com/devzone/conceptd.nsf/webmain/8CA8DE2E8881C1AB8625682E0079CE74.

objects upon which it is operating, particularly when iterative procedures are followed.

Following successful processing of the aggregate mask, the fine aggregate particles can be removed by simple morphological operations and can be saved as a separate, dedicated, fine aggregate binary mask. The production of separate coarse and fine aggregate binary masks is very useful when performing advanced image measurement, particularly when compensations are required to allow for the effects of fine aggregate interfacial development, on HCP microstructure when investigating coarse aggregate interfacial characteristics. For example the investigator may wish to discount measurements of ITZ, or HCP characteristics, *after* (say) a distance beyond the midpoint between the two particles is reached. It is therefore possible to imagine a boundary that follows the exact midpoint distances between the coarse aggregate interface and any fine aggregate interfaces that fall within the desired area of measurement.

3.2. Production of porosity and coarse aggregate masks for measurement and image processing

The next step involves production of a porosity mask from thresholding of the BEI (Fig. 8a). Here, a range of pixels that correspond to the resin filled voids of the image are selected based on their greyscale values. For these features, corresponding pixels are black or very close to black, resulting from a low backscattered signal coefficient generated by interaction of the electron beam with the very low atomic number resin. Greyscale values for these coefficients are therefore located in the lower value regions to the left of the image greyscale histogram (illustrated in Fig. 8b).

For this exercise a threshold value of 42 was selected to identify the porosity content of the image from Fig. 1a, which is the median greyscale value between the maximum peak values for C–S–H and porosity present in the HCP curve of the diagram as shown in Fig. 8b. The assumption is that pixels located mid-way between peaks represent pixels comprising of 50% signal from one of the phases and 50% signal from the other phase, and are therefore a logical choice for thresholding [6]. Problems exist however, in regions where multi peak overlap exists, requiring advanced deconvolution processing to be performed. In the case of the porosity and C–S–H peaks shown here though, this complication does not exist. There are, in fact, several different methods used by various researchers in an attempt to avoid subjective manual selection of a threshold value and the inherent biases introduced as a result. For example Scrivener et al. [7] adopted a method where tangents that represent the initial grey value slopes of the histogram, and the hydration products peak, intersect at a point that closely matched the manual threshold value and gave consistent results. Yang and Buenfeld [8] however, produced an algorithm for direct segmentation of aggregate particles from BEI's, using an edge detection filter. This has the advantage of ignoring global greyscale values for thresholding purposes, instead taking advantage of local gradient differences to define edges,

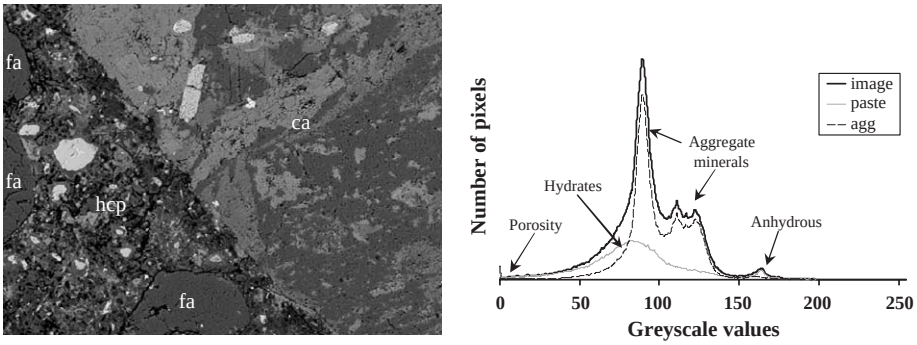

a) BEI of coarse aggregate (ca), fine aggregate (fa) and hardened cement paste (hcp)

b) Histogram of a) showing distribution of image components

Fig. 8. BEI and corresponding greyscale histogram for constituent fractions of image.

although later post-processing of binary images may remove smaller aggregate particles from the image. Recent work undertaken within the Concrete Durability Group at Imperial College is being prepared for review prior to publication, and represents a further contribution to greyscale thresholding of hardened concrete backscattered electron images [9].

After thresholding of porosity values, the resulting binary mask is processed to improve accuracy of both porosity and coarse aggregate masks. First, the porosity mask is subtracted from the coarse aggregate mask to allow for any interfacial morphological overlap, which may have been introduced into the coarse aggregate mask from the 'smoothing' (filtering) operation performed during its creation. This ensures that any odd pixel representing smaller pores lying at the aggregate interface will not be 'lost' during measurement. The coarse aggregate mask is reprocessed to fill any holes, and to remove any noise introduced during subtraction of the porosity mask, and is re-saved ready for image analysis measurement routines. The new coarse aggregate mask and the previously created fine aggregate mask are both subtracted from the porosity mask, so that a new image is produced for HCP-only porosity. The final two masks used for measurement of interfacial porosity on the example image provided in Fig. 1 are shown in Fig. 9.

3.3. Image quantification (measurement)

To measure the distribution of interfacial porosity, the coarse aggregate is dilated and subtracted from its previous size to create an interfacial strip of known dimensions. This process is repeated leading to the formation of multiple strips lying on top of each other with progressive distance from the coarse aggregate interface. Each one of these strips is then combined with the porosity mask through the use of a logical operator. This method of measuring interfacial porosity is a technique first used by Scrivener and Gartner [1] to characterise the nature of porosity, hydration products, and anhydrous material in close proximity to the coarse aggregate interface, in the so-called interfacial transition zone (ITZ). They produced 'bands' that were 3 μm wide around aggregate particle interfaces. The technique has now become routinely used in the analysis of backscattered electron micrographs, although resolution, thickness and therefore accuracy of the interfacial strips tend to vary between researchers. For example Diamond [10] and Diamond and Huang [11], used bands of 10 μm intervals. In these studies it is claimed that (within the 10 μm bands) there *appeared* to be no significant difference in the amount of porosity measured between the 0–5 μm portions, and the 5–10 μm portions. It might be argued, however, that a 'micro profile' may exist within bands of such relatively large dimensions.

In this study, scaling of images (pixel size calibration) produced pixel sizes of 1.19 μm, with individual surface areas of 1.42 μm^2. In view of this, it was felt that interfacial strips two pixels wide would be adequate for measurement purposes, and would produce interfacial strips 2.4 μm wide. To achieve this, the coarse aggregate mask is grown or dilated by two pixels, using a hexagonal morphological filter as described above. The original mask is then subtracted from the new to produce an interfacial strip. This strip is combined with the porosity mask using a logical 'AND' operator, so that only pixels of matching positions on both images are preserved. The new pixel 'map' represents features of interest (porosity) that lie within 2.4 μm of the previous datum line (i.e. the coarse aggregate interface or previous interfacial strip), which are measured and calculated as a percentage of the total strip area. This procedure is repeated consecutively for a required distance into the HCP, and can be represented graphically as a profile of measured values with distance from the interface. A series of contours or 'isopachs' (lines of equal value) can also be drawn onto the image representing the perimeter of each strip, and showing the area covered by each-iteration of the measurement program.

The strips can be combined with other segmented masks that could represent other fractions of the material such as hydrate phases (CH, C–S–H), air voids, cracks, anhydrous material, small aggregate particles, in fact any feature that is capable of being accurately segmented from the BEI. It is also possible to calculate porosity as a percentage of the total paste area of the image, by combining the aggregate corrected porosity mask with the inverted aggregate-only, binary mask image. Before deducting the porosity mask image from the coarse aggregate mask, porosity values for the first interfacial measurement strip were calculated at approximately 7%. This

a) Porosity mask (threshold greyscale values 0-42) b) Coarse aggregate mask (porosity adjusted at interface)

Fig. 9. Final porosity mask and coarse aggregate mask to be used in measurement routines.

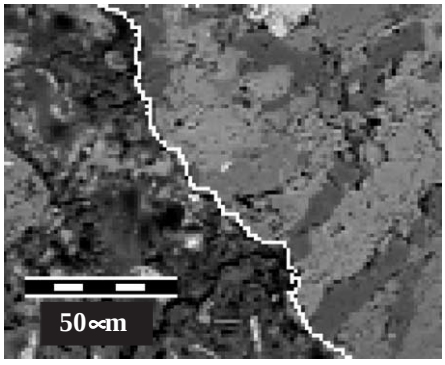

a) Central area of Fig 1a (zoomed) showing fit of coarse aggregate binary mask around the particles' interface

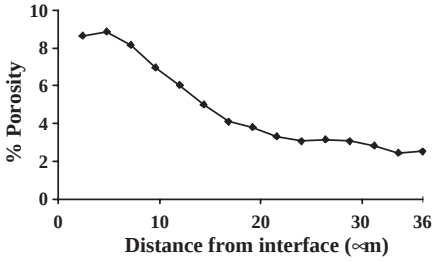

b) Plot of porosity with distance from the interface (average of 30 data sets)

Fig. 10. Results of image analysis of interfacial strips.

means that the true porosity value for the area immediately adjacent to the interface would have been underestimated by about 2%, and for systems with a higher porosity content, this figure could have been significantly higher. In order to arrive at a statistically reliable figure, it is normal for many images to be measured.

The image presented in Fig. 10a demonstrates the accuracy of the technique. Close inspection of the fit of the mask to the particle interface shows the line to lie within one pixel (or 1.2 μm) of the interface. Fig. 10b presents the results calculated from 30 image data sets, which were analysed by semi automated software macro programs. Standard deviations for the measured porosity are provided in Table 1.

A reduction in porosity with distance from the coarse aggregate interface is evident and generally in line with published literature (Scrivener et al. [2]; Diamond [10]; Diamond and Huang [11]; Scrivener and Nemati [12]) of approximately 8–9% immediately adjacent to the interface, reducing to 2% or 3% at a distance of 36 μm from the interface. There is also a reduction in measured strip size with distance from the interface, which is due to the angular loss of strips as they get farther away from the interface, and from encountering particles of fine aggregate. This reduction in the strip size was calculated at about 18% over the distance measured. The strips also become 'smoother' as interfacial irregularities are 'ironed out' by repetitive filtering.

This technique is valid for a range of multi-phase (mineral) aggregate types, where it is possible to assign elements to particular mineral phases of the aggregate. For example, granite is also widely used as crushed natural aggregate, and is composed mainly of silica rich minerals such as quartz and feldspars often in association with accessory mafic minerals such as hornblende (an amphibole) and biotite (a mica). In this case Na, Mg, Al, K, Si, and Fe might be the preferred primary use dot map images used for construction of the aggregate particle binary mask, although Ca might help to identify the hornblende. It has also been stated however, that where Ca-rich phases lie in contact with the aggregate/HCP interface, a combination of minor element dot maps may be used in replacement of the Ca dot map for the construction of this phase. The range of possible elements present can be quite extensive therefore, requiring careful selection of the most useful elemental dot maps for later binary mask construction.

Table 1
Calculated porosity (avg. 30 data sets) and standard deviations (% per strip)

Strip no.	1	2	3	4	5	6	7	8	9	10	11	12	13	14	15
Porosity	8.7	8.9	8.2	7.0	6.0	5.0	4.1	3.8	3.3	3.1	3.2	3.1	2.8	2.4	2.5
S.D.	7.6	8.0	7.0	5.4	4.7	4.1	3.4	3.0	3.0	3.2	3.2	3.3	3.5	2.7	2.7

4. Conclusions

A method for combining scanning electron microscopy, and energy dispersive X-ray imaging to accurately identify complex aggregate interfaces with the cement paste in a hardened concrete has been presented. It involves the identification of aggregate chemical composition by collection of X-ray spectra, then backscattered image capture simultaneous with X-ray dot map data capture, and subsequent image processing and quantification by advanced image analysis software algorithms. It can cope with aggregate that is composed of different mineral phases with different greyscale intensities. The resulting aggregate mask is able to be used in image analysis routines, allowing for BEI features such as porosity to be segmented and measured. Other features that could be measured include the hydrate phases, anhydrous phases, fine aggregate particles and cracks.

The work presented has concentrated on providing a step-by-step summary of the different stages of image processing. To obtain quantified results it is necessary to apply the technique to large data sets. This will inevitably require some level of (semi) automation of image analysis routines, such that repetitive operations can be standardised, so by speeding up data processing and removing potential operator biases. Attention has also been given to small binary mask image adjustments that are sometimes necessary to achieve better accuracy of measured results.

Acknowledgements

The authors would like to acknowledge EPSRC for support under grant GR/M97206, and for equipment funding under grant GR/S18175.

References

[1] K.L. Scrivener, E.M. Gartner, in: S. Mindess, S.P. Shah (Eds.), Bonding in Cementitious Composites, vol. 114, Materials Research Society, Pittsburgh, USA, 1988, p. 77.
[2] K.L. Scrivener, A.K. Crumbie, P.L. Pratt, in: S. Mindess, S.P. Shah (Eds.), Bonding in Cementitious Composites, vol. 114, Materials Research Society, Pittsburgh, USA, 1988, p. 87.
[3] E. Backstrom, S. Hansen, Adv. Cem. Res. 9 (33) (1997) 17.
[4] A.R. Brough, A. Atkinson, Cem. Conc. Res., vol. 30, Pergamon Press Inc., USA, 2000, p. 849.
[5] P. Stutzman, Cement and Concrete Composites, vol. 26, Elsevier, 2003, p. 957.
[6] M.K. Head, Influence of the interfacial transition zone (ITZ) on the properties of concrete. PhD Thesis. University of Leeds. UK, 2001.
[7] K.L. Scrivener, H.H. Patel, P.L. Pratt, L.J. Parrott, Materials Research Society Symposium—Proceedings, vol. 85, Materials Research Society, Pittsburgh, USA, 1987, p. 67.
[8] R. Yang, N.R. Buenfeld, Cem. Conc. Res., vol. 31, Pergamon Press Inc., USA, 2001, p. 437.
[9] H.S. Wong, M.K. Head, N.R. Buenfeld. Cem. Concr. Res. (in press), doi:10.1016/j.cemconres.2005.10.006.
[10] S. Diamond, Cement and Concrete Composites, vol. 23, Elsevier, 2001, p. 171.
[11] S. Diamond, J. Huang, Cement and Concrete Composites, vol. 23, Elsevier, 2001, p. 179.
[12] K.L. Scrivener, K.M. Nemati, Cem. Conc. Res., vol. 26 (1), Pergamon Press Inc., USA, 1996, p. 35.